MITSUBISHI ELECTRIC RESEARCH LABORATORIES
http://www.merl.com

Polarized MIMO Channels in 3-D: Models, Measurements and Mutual Information

Mansoor Shafi, Min Zhang, Aris L. Moustakas, Peter J. Smith, Andreas F. Molisch, Fredrick Tufvesson, Steven H. Simon

TR2006-020 March 2006

Abstract

4G systems are expected to support data rates of the order of 100 Mbps in the outdoor environment and 1 Gbps in the indoor/stationary environment. In order to support such large payloads, the radio physical layer must employ receiver algorithms that provide a significant increase in spectrum efficiency (and hence capacity) over current wireless systems. Recently an explosion of MIMO studies have appeared with many journals presenting special issues on this subject. This has occured dur to the potential of MIMO to provide a linear increase in capacity with antenna numbers. Environmental conciderations and tower loads will often restrict the placing of large antenna spans on base stations. Similarly, customer device form factors also place a limit on the antenna numbers that can be placed with a mutual spacing of 0.5 wavelength. The use of cross-polarized antennas is widely used in modern cellular installtions as it reduces spacing needs and tower loads on base stations. Hence, this approach is also receiving considerable attention in MIMO systems. In order to study and compare various receiver architectures that are based on MIMO techniques, one needs to have an accurate knowledge of the MIMO channel. However, very few studies have appeared that characterize the cross-polarized MIMO channel. Recently, the third generation partnership standards bodies (3GPP/3GPP2) have defined a cross-polarized channel model for MIMO systems but this model neglects the elevation spectrum. In this paper we provide a deeper understanding of the channel model for cross-polarized systems for different environments and propose a composite channel impulse model for the cross-polarized channel that takes into account both azimuth and elevation spectrum. We use the resulting channel impulse response to derive closed form expressions for the spatial correlation. We also present models to describe the dependence of cross-polarization discrimination (XPD) on distance, azimuth and elevation and delay spread. In addition, we study the impact of array width, SNR and antenna slant angle on the mutual information (MI) of the system. In particular we present an analytical model for large system mean mutual information values and consider the impact of elevation spectrum on MI. Finally, the impace of multipath delays on XPD and MI is also explored.

IEEE Journal on Selected Areas in Communications

MITSUBISHI ELECTRIC RESEARCH LABORATORIES
http://www.merl.com

Polarized MIMO Channels in 3-D: Models, Measurements and Mutual Information

Mansoor Shafi, Min Zhang, Aris L. Moustakas, Peter J. Smith, Andreas F. Molisch, Fredrick Tufvesson, Steven H. Simon

TR2006-020 March 2006

Abstract

4G systems are expected to support data rates of the order of 100 Mbps in the outdoor environment and 1 Gbps in the indoor/stationary environment. In order to support such large payloads, the radio physical layer must employ receiver algorithms that provide a significant increase in spectrum efficiency (and hence capacity) over current wireless systems. Recently an explosion of MIMO studies have appeared with many journals presenting special issues on this subject. This has occured dur to the potential of MIMO to provide a linear increase in capacity with antenna numbers. Environmental conciderations and tower loads will often restrict the placing of large antenna spans on base stations. Similarly, customer device form factors also place a limit on the antenna numbers that can be placed with a mutual spacing of 0.5 wavelength. The use of cross-polarized antennas is widely used in modern cellular installtions as it reduces spacing needs and tower loads on base stations. Hence, this approach is also receiving considerable attention in MIMO systems. In order to study and compare various receiver architectures that are based on MIMO techniques, one needs to have an accurate knowledge of the MIMO channel. However, very few studies have appeared that characterize the cross-polarized MIMO channel. Recently, the third generation partnership standards bodies (3GPP/3GPP2) have defined a cross-polarized channel model for MIMO systems but this model neglects the elevation spectrum. In this paper we provide a deeper understanding of the channel model for cross-polarized systems for different environments and propose a composite channel impulse model for the cross-polarized channel that takes into account both azimuth and elevation spectrum. We use the resulting channel impulse response to derive closed form expressions for the spatial correlation. We also present models to describe the dependence of cross-polarization discrimination (XPD) on distance, azimuth and elevation and delay spread. In addition, we study the impact of array width, SNR and antenna slant angle on the mutual information (MI) of the system. In particular we present an analytical model for large system mean mutual information values and consider the impact of elevation spectrum on MI. Finally, the impace of multipath delays on XPD and MI is also explored.

IEEE Journal on Selected Areas in Communications

Polarized MIMO Channels in 3D: Models, Measurements and Mutual Information

Mansoor Shafi, Min Zhang, Aris L. Moustakas, Peter J. Smith, Andreas F. Molisch, Fredrik Tufvesson and Steven H. Simon

Abstract

4G systems are expected to support data rates of the order of 100 Mbps in the outdoor environment and 1 Gbps in the indoor/stationary environment. In order to support such large payloads, the radio physical layer must employ receiver algorithms that provide a significant increase in spectrum efficiency (and hence capacity) over current wireless systems. Recently an explosion of MIMO studies have appeared with many journals presenting special issues on this subject. This has occured due to the potential of MIMO to provide a linear increase in capacity with antenna numbers. Environmental considerations and tower loads will often restrict the placing of large antenna spans on base stations. Similarly, customer device form factors also place a limit on the antenna numbers that can be placed with a mutual spacing of 0.5 wavelength. The use of cross-polarized antennas is widely used in modern cellular installations as it reduces spacing needs and tower loads on base stations. Hence, this approach is also receiving considerable attention in MIMO systems. In order to study and compare various receiver architectures that are based on MIMO techniques, one needs to have an accurate knowledge of the MIMO channel. However, very few studies have appeared that characterize the cross-polarized MIMO channel. Recently, the third generation partnership standards bodies (3GPP/3GPP2) have defined a cross-polarized channel model for MIMO systems but this model neglects the elevation spectrum. In this paper we provide a deeper understanding of the channel model for cross-polarized systems for different environments and propose a composite channel impulse model for the cross-polarized channel that takes into account both azimuth and elevation spectrum. We use the resulting channel impulse response to derive closed form expressions for the spatial correlation. We also present models to describe the dependence of cross-polarization discrimination (XPD) on distance, azimuth and elevation and delay spread. In addition, we study the impact of array width, SNR and antenna slant angle on the mutual information (MI) of the system. In particular we present an analytical model for large system mean mutual information values and consider the impact of elevation spectrum on MI. Finally, the impact of multipath delays on XPD and MI is also explored.

Index Terms

MIMO, cross-polarized channels, capacity.

I. Introduction

The use of cross-polarized antennas for multiple-input-multiple-output (MIMO) systems is now receiving considerable attention. It is well known that for a fixed ratio of transmit to receive antenna numbers, and under certain channel conditions MIMO system capacity can be linearly proportional to the minimum of the number of transmit and receive antennas. Cross-polarized systems are of interest since they are able to double the antenna numbers for half the spacing needs of co-polarized antennas. Slant polarized antennas are already used for cellular mobile systems for up link receive diversity and are therefore potential candidates for use on systems that use MIMO receivers. Very few studies are available on propagation models for cross-polarized channels. The papers most often cited are those of [1], [2].

Mansoor Shafi is with Telecom New Zealand Ltd, 49-55 Tory Street, Wellington, New Zealand, email: Mansoor.Shafi@telecom.co.nz

Min Zhang and Peter J. Smith are with the Department of Electrical and Computer Engineering, University of Canterbury, Private Bag 4800, Christchurch, New Zealand, email: mzh22@student.canterbury.ac.nz, p.smith@elec.canterbury.ac.nz

Aris L. Moustakas and Steven H. Simon are with Lucent Technologies, Bell Labs, 600 Mountain Ave., Murray Hill, NJ 07974, USA, email: arislm,shsimon@lucent.com

Andreas F. Molisch is with Mitsubishi Electric Research Labs, Cambridge, MA, USA, and the Department of Electroscience, Lund University, Box 118, SE-221 00 Lund, Sweden, email: andreas.molisch@ieee.org

Fredrik Tufvesson is with the Department of Electroscience, Lund University, Box 118, SE-221 00 Lund, Sweden, email: fredrik.tufvesson@es.lth.se

However both these papers consider only transmission from a vertically polarized antenna and also do not consider the impact of elevation spectrum.

For mobile terminals located in indoor buildings and in vehicles, the elevation spectrum must also be considered. There is a real scarcity of published models for the elevation spectrum in the environments that are suitable for MIMO system studies. In a study done in urban Tokyo [3], a Gaussian elevation spectrum is proposed and measurements are used to derive an expression for the mean effective gain of a mobile antenna. In a recent study [4] the elevation spectrum and cross-polarization discrimination (XPD) were measured in different radio propagation environments in Finland. In another recent study done under the auspices of the 3GPP and 3GPP2, a cross-polarized channel model for MIMO systems was developed [5], but the elevation spectrum impacts are neglected.

In this paper we make the following contributions:

- We present a comprehensive model for the cross-polarized channel and extend the 3rd Generation Partnership Project (3GPP) model to include a three-dimensional (3D) component. We call this the composite channel.
- We discuss a model for XPD and discuss its dependence on distance, angles and delay spread, partly derived from a new measurement campaign.
- Using the composite channel, we develop closed form expressions for spatial correlations and verify their accuracy by simulations. The overall spatial correlation is a weighted sum of the constituent 2D and 3D components. We also show that when the angles of arrival and departure are dependent on each other and follow a von-Mises distribution [6], the spatial correlation can be written in a sum-Kronecker form.
- Using the composite channel we determine the ergodic mutual information (denoted as MI) by simulation and study the impact of XPD and antenna slant angle. In order to show the benefits of using cross-polarized antennas we compare the MI values obtained by cross-polarized and co-polarized antennas for similar total array sizes. We also determine analytic expressions for large system MI values and verify their accuracy by comparing them to the simulations.
- Finally we look at the impact of the delay-dependence of the XPD on the system capacity in frequency selective fading.

Results show that system MI is very sensitive to the relative proportions of the 2D and 3D components especially when the signals arriving to the mobile have a low angle spread. The closed form spatial correlations derived are shown to give good agreement to the more complex models in [7]. Large system approximations to the MI values under these correlation scenarios are also shown to be very accurate. The XPD measurements are used to develop models of XPD vs distance and delay and simulations of the relationship between MI and the temporal dependence of XPD suggest the effects are minor.

The paper is organized as follows. Section II develops the new generalized composite channel model and Section III reviews the literature on XPD before presenting new XPD measurements. Section IV derives the correlation structure for the new model. Results and conclusions are given in Sections V and VI.

II. Generalized Model For Cross-Polarized Channels

In this section we will briefly describe the Spatial Channel Model (SCM) introduced in [5] and subsequently generalize it to take into account the effects of three-dimensional (3D) propagation and polarization mixing, in particular, for indoors and in-vehicle situations.

A. 2D simplified SCM model

The SCM model is a detailed system level model for a variety of environments. It does not consider the elevation spectrum; therefore it is defined for the two dimensional (2D) case. The SCM considers N clusters of scatterers and each simulation, or drop, varies the cluster statistics and array orientations. A

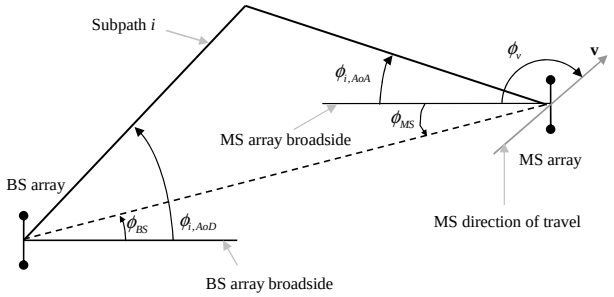

Fig. 1. Simplified SCM model for 2D case

cluster corresponds to a separate path and within the path, there are M unresolvable subpaths (M equals 20 for SCM). A simplified sketch of the model is given in Fig. 1.

The largely 2D character of electromagnetic propagation in outdoors environments, with about $1-2^o$ elevation spread at the base-station [8], has an important implication in the modeling of the propagation and mixing of the polarization of electromagnetic waves. Specifically, one can decompose the polarization into vertical and in-plane directions. Also, while the in-plane (horizontal) components tend to mix with each other strongly, the mixing between horizontal and vertical components generally is relatively small, with a path XPD ratio typically larger than 6dB. Therefore, in general one needs to model four channels between base and mobile antennas, namely those connecting the horizontal/vertical polarization at the base-station to the horizontal/vertical polarization at the mobile station. This results in the decomposition of the antenna patterns at both ends into vertical and horizontal. Throughout the paper we assume ideal tilted dipole antennas both for the 2D and 3D cases. We also assume all the polarization mixing is due to the path effects i.e., we neglect antenna polarisation leakage effects. Thus, for example, an ideal dipole antenna with polarization vector $\mathbf{p}$ tilted at angle α from the z-axis (see Fig. 2), has vertical and horizontal components of the antenna pattern which are proportional to

$$\boldsymbol{\chi}(\mathbf{k}) = \begin{bmatrix} \chi^v(\mathbf{k}) \\ \chi^h(\mathbf{k}) \end{bmatrix} e^{i\mathbf{kr}} = \begin{bmatrix} \cos\alpha \\ \sin\alpha\cos\phi \end{bmatrix} e^{i\mathbf{kr}} \tag{1}$$

where for compactness we have included the overall phase factor for the incoming wave in the response of the antenna. $\mathbf{r}$ is the vector signifying the position of the antenna with respect to the center of the antenna array. The actual position of the center of the array is not important, since as we shall see later, only relative distances between antennas will play a role in the model. The vector $\mathbf{k}$, defined by

$$\mathbf{k} = 2\pi/\lambda[\cos\phi, \sin\phi, 0] \tag{2}$$

is the 3D wave-vector of the direction of the incoming (or outgoing) wave, with the carrier wavelength λ and ϕ is the azimuth angle of incoming/outgoing waves.

For simplicity, we focus on a single path. The fading channel coefficient $h_{su}^{2D}(t)$ of the path between base-station (BS) antenna s and mobile-station (MS) antenna u as given in [5] is then given by

$$h_{su}^{2D}(t) = \sqrt{\frac{1}{M}} \sum_{i=1}^{M} \left(\boldsymbol{\chi}_{s,BS}^{\dagger}(\mathbf{k}_{i,BS}) \mathbf{H}_i^{2D} \boldsymbol{\chi}_{u,MS}(\mathbf{k}_{i,MS}) e^{-i\mathbf{k}_{i,MS}\cdot\mathbf{v}t} \right) \tag{3}$$

with the superscript ^{2D} indicating wave propagation in 2 dimensions. In the above, $\boldsymbol{\chi}$ are the antenna response vectors for the BS and MS antennas as defined in (1). It should be stressed that this equation is valid for arbitrary antenna patterns, not necessarily, ideal dipole antennas. Note that the square norm of $\boldsymbol{\chi}$, $G(\mathbf{k}) = |\boldsymbol{\chi}(\mathbf{k})|^2$, is the antenna gain in the direction $\mathbf{k}$. Also, $\mathbf{k}_{i,MS}$ and $\mathbf{k}_{i,BS}$ in (3) are the random plane wavevectors of the incoming and outgoing waves for each wave component $i = 1, ..., M$, both assumed

to be in the horizontal plane. $\mathbf{v}$ is the velocity vector of the mobile and t is time. In addition, $\mathbf{H}_i^{2D}$ is a 2×2 matrix containing the random coefficients of the $i = 1, \ldots, M$ wave components given by

$$\mathbf{H}_i^{2D} = \begin{bmatrix} z_i^{vv} & \sqrt{r_1} z_i^{vh} \\ \sqrt{r_2} z_i^{hv} & z_i^{hh} \end{bmatrix}. \tag{4}$$

The z_i terms in (4) are the random coefficients of the ith wave component of the sum for each of the four polarization channels HH, HV, VH, VV. In the SCM model [5], these terms are defined as iid complex exponentials instead of complex Gaussians, for computational efficiency. Hence, if exact Rayleigh channels are desired, the z_i terms can be defined as iid complex Gaussians. Otherwise, iid complex exponentials can be used. In the results shown in this paper iid complex exponentials are used, except in the large sample results where an exact Rayleigh channel is assumed. r_1 and r_2 are the inverse XPD values for VV/VH and HH/HV respectively. In other words, r_1 is the power of the VH component relative to the VV component. Note that the fading of the channel component $h_{su}^{2D}(t)$ is manifested by the movement of the mobile with respect to the ground. The incoming plane-waves $\mathbf{k}_{MS}$ are assumed to be coming from fixed sources toward the mobile.

Finally we point out that for fixed total transmitted power, the total received power increases as a function of decreasing XPD. This is to be expected because the vertical component receives power due to mixing from the horizontal component and vice-versa. As a matter of convention, as we vary the XPD, we will assume fixed transmitted power rather than fixed received power. This is also the convention adopted in [5].

B. 3D SCM model

The assumption of 2D propagating waves breaks down when in some propagation environments the angular spectrum is significant. This effect is particularly important when analyzing cross-correlations between antennas with very different 3D response patterns. In these cases, focusing only on the radiation arriving in the horizontal plane may produce erroneous results. Therefore, we need to modify the above 2D model to incorporate such effects. In doing so, we should aim to minimize the increase in complexity by the introduction of parameters describing the 3D character of the radiation at the mobile. Since the existing two-dimensional model captures many of the effects of outdoors propagation we would like to extend it to cases where the mobile antennas are located at indoor and in-vehicle environments. Both of these cases are characterized by nearly uniform spherical radiation to the mobile.

Very few measurements of elevation spectrum are available in the open literature. Therefore we make some simplifying assumptions about the elevation spectrum that enable us to develop closed form expressions for the 3D spatial correlation.

The first step in modeling the 3D channel is to take into account the full three-dimensional antenna response of the mobile antennas, by expressing the response vector $\boldsymbol{\chi}$ in its θ and ϕ components:

$$\boldsymbol{\chi}_{MS}(\mathbf{k}) = \begin{bmatrix} \chi^{\theta}(\mathbf{k}) \\ \chi^{\phi}(\mathbf{k}) \end{bmatrix} = \begin{bmatrix} \cos\alpha \sin\theta + \sin\alpha \cos\theta \sin\phi \\ \sin\alpha \cos\phi \end{bmatrix} e^{i\mathbf{kr}} \tag{5}$$

where χ^{θ}, χ^{ϕ} are the θ and ϕ polarized responses of the antenna at direction $\mathbf{k}$. The vector $\mathbf{k}$ is defined in terms of θ and ϕ as [3], [9]:

$$\mathbf{k} = 2\pi/\lambda[\sin\theta\cos\phi, \sin\theta\sin\phi, \cos\theta] \tag{6}$$

as shown in Fig. 2. Note that in the limit of horizontal wave propagation, i.e., when $\theta = \pi/2$, we recover the form of antenna response shown in (1).

The relative strength of the 3D radiation at the mobile to that of the already existing 2D radiation depends on several factors, including the distance of the mobile from openings (e.g. windows). Since the surfaces from which these waves emanate towards the mobile are of no particular geometry, we expect the horizontal and vertical components of the radiation to have been fully mixed, and therefore

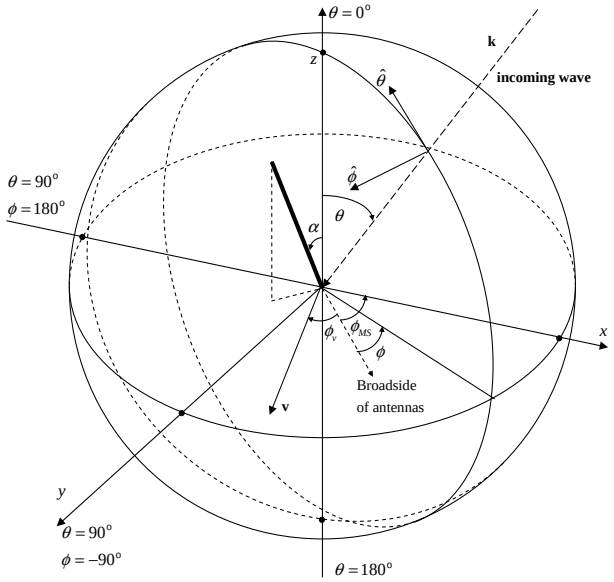

Fig. 2. Spherical coordinate system for 3D model

the corresponding XPD for these processes are assumed to be equal to unity. It should be noted that the accuracy of this statement depends on the bandwidth of the signal. For bandwidths up to 100Mhz, due to strong mixing of all paths, the XPD can be assumed to be unity. For very wide frequency bands, with correspondingly short symbol durations, a lot more individual paths are distinguishable, and therefore the XPD per path is expected to be higher. However, for bandwidths up to 100MHz [10] the uniform distribution in the elevation spectrum in the absence of line-of-sight is a good approximation. As a result, we may write the fading channel coefficient $h_{su}^{3D}(t)$ for this component of the propagation between BS antenna s and MS antenna u as

$$h_{s,u}^{3D}(t) = \sqrt{\frac{1}{M}} \sum_{i=1}^{M} \left(\boldsymbol{\chi}_{s,BS}^{\dagger}(\mathbf{k}_{i,BS}) \mathbf{H}_i^{3D} \boldsymbol{\chi}_{u,MS}(\mathbf{k}_{i,MS}) e^{-i\mathbf{k}_{i,MS}\cdot\mathbf{v}t} \right) \tag{7}$$

with the superscript ^{3D} indicating wave propagation in 3 dimensions. The $\mathbf{k}_{i,MS}$ are independently chosen for the 2D and 3D channel coefficients and the matrix $\mathbf{H}_i^{3D}$ for the ith wave component is given by

$$\mathbf{H}_i^{3D} = \begin{bmatrix} z_i^{v\theta} & z_i^{v\phi} \\ z_i^{h\theta} & z_i^{h\phi} \end{bmatrix} \tag{8}$$

The z_i terms in (8) are the random coefficients of the ith wave component of the sum for each of the V and H channels and their respective components in the θ and ϕ polarizations respectively. The definition of the z_i terms is discussed below (4). The antenna responses $\boldsymbol{\chi}$ for the BS are the same for both 2D and 3D models. At the MS, the antenna responses are different due to the 3D character of the radiation. As in the case of (3), equation (7) is valid for arbitrary antenna patterns, described by $\boldsymbol{\chi}_{s,BS}$ and $\boldsymbol{\chi}_{u,MS}$. Nevertheless, for concreteness we focus on the simple case of ideal dipole antennas.

Assuming that the composite channel consists of two independent terms namely the 2D and 3D channel coefficients, scaled by their relative powers. We can use the 2D and 3D channel coefficients to model a composite channel coefficient. Thus, we can write the composite channel coefficient between antennas s and u as

$$h_{su}(t) = \sqrt{\frac{1}{1+g}} h_{su}^{2D}(t) + \sqrt{\frac{g}{1+g}} h_{su}^{3D}(t) \tag{9}$$

where g is the ratio of powers of the 3D to 2D components of the channel. There are very few measurements of g. For the case of indoor mobiles, which are far from open spaces, e.g. windows, one can

assume that $g = \infty$, i.e., one can keep only the 3D components of the channel. For indoor channels close to a window, a reasonable value for g is $g = -4dB$ [11]. A similar is assumed for in-vehicle mobiles.

III. Models and Measurements for XPD

As shown in (3) and (4), the polarization mixing for the entire path is governed by the inverse XPD values r_1 and r_2. Most models make the assumption that $r_1 = r_2$, or more explicitly, that $VV = HH$ and $VH = HV$. While this might be an oversimplification, only a few measurements are available that do not make this assumption. In this section, we discuss measurements and statistical models for the XPD in the literature, as well as the results from a new measurement campaign.

There is a general consensus in the literature that the XPD, when expressed in dB, has a non-zero-mean Gaussian distribution (though many papers only give a mean and variance, without analyzing the exact shape, or giving a goodness-of-fit test). Hence, we may write $XPD \sim \mathcal{N}(\mu, \sigma)$.

Depending on the environment and the existence of a line-of-sight (LOS) connection, the mean XPDs measured in the literature vary from 0 to 18dB, with standard deviations typically of the order of 3-8 dB.

From the physical propagation processes, we can also conclude that the XPD can depend on other channel parameters, namely the total attenuation (or equivalently, the distance between transmitter and receiver), the angles of arrival and departure (both azimuth and elevation), as well as the delay of the multipath components. We first review the literature for measurements of those dependencies, and then present measurement results in an indoor environment. From the results, we can obtain XPD values that are relevant for different environments, distances, and delays. These values can then be used, for example, in the MI computations of Section V.

1) Dependence of XPD on distance: For indoor environments, extensive measurements are given in [12]. These authors found that for a corridor environment with LOS, the decay with distance can best be modeled as an exponential decay, although the traditional $n \log(d)$ law also gives satisfactory performance. Decay exponents are different for all polarizations, namely 1.07, 1.20, 1.49 and 1.47 for VV, HH, VH and HV respectively. The XPD is large (around 15 dB), and increases with distance. Other indoor measurements are reported by [13], [14]. For outdoor environments, distance dependence of XPD measurements are reported by [15], [16], [17], and [4].

2) Dependence of the XPD on azimuth and elevation: In [18], measurements were performed with vertically and horizontally polarized antennas of different antenna patterns, and a definite dependence of XPD on antenna pattern was found. However, it is difficult to extract azimuth and/or elevation-dependent XPDs from these results.

For macrocells, results in [19] suggest that the azimuth spread is independent of the polarization when the polarization directions $\pm 45^\circ$ are considered. However, for vertical transmission from the MS, the XPD has been shown to have a weak ($\rho = -0.15$) negative correlation with the azimuth spread [20]; in other words, a larger azimuth spread at the base leads to a lower XPD. Again, this result is intuitive, as a larger azimuth spread indicates stronger scattering.

Extensive investigations of the elevation at the mobile station, and its dependence on the polarization can be found in [4]. For simplicity, in the case of indoor and in-vehicle environments we assume that the elevation spectrum is such that every point on the sphere in Fig.2 is equally likely and the elevation spectrum for both polarizations is the same.

3) Dependence of XPD on delay spread: Results in [21] and [20] did not find a dependence between delay spread and polarization in outdoor environments. A similar result was obtained for indoor environments by [13]. However, some of the measurements in [20] showed a difference in the shape of the power delay profile for the two polarizations.

In [22] it was found that the co-polarized and cross-polarized components had different decay time constants. Analyzing cluster decay constants in a microcellular scenario, they showed that the VV component decayed with 8.9 dB/μs, while the co-polarized component decayed with 11.8 dB/μs. This indicates that the XPD *increases* with increasing delay - a somewhat surprising result. However, the 3GPP model finds

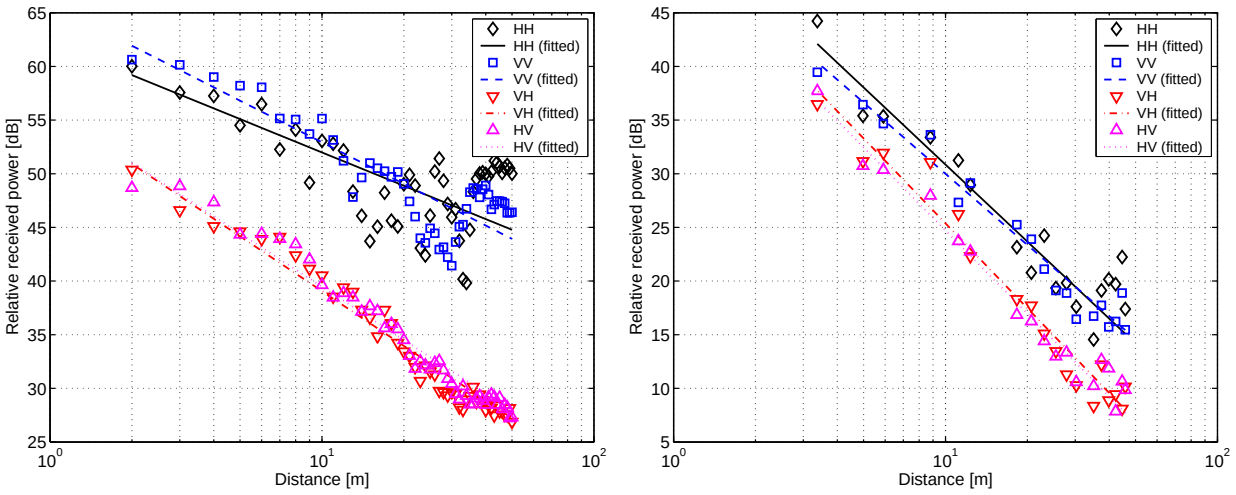

(a) a corridor LOS scenario

(b) a corridor NLOS scenario

Fig. 3. Power of the different polarization components as a function of distance

for macrocellular environments that the mean (in dB) is equal to $0.34 * (\text{mean relative path power in dB}) + 7.2$ so that the XPD decreases with increasing delay; in microcellular environments, the XPD is a constant $8dB$.

A. XPD Measurements

Here we briefly report on the measurements that were performed with the RUSK LUND MIMO channel sounder from MEDAV at a center frequency of 2.6 GHz and a bandwidth of 200MHz. Due to limitations of space we are unable to report on the measurement set up, details can be found in [23]. We have measured two indoor office scenarios at various distances: LOS in a corridor and NLOS between the corridor and the offices, where the walls consist mainly of gypsum wallboards. We evaluated the measurement results to obtain the entries of the polarization matrix, both as a function of the distance, and as a function of the delay. Fig. 3 shows the power of the different components P^{vv}, P^{vh}, P^{hv}, and P^{hh} with the best fitting linear curves as a function of the distance. The curves are obtained by the minimum squared error integrated over the logarithm of the distance. Fig. 3(a) shows the results for the LOS scenario. Similarly, Fig. 3(b) shows the results for the corridor-to-office (NLOS) scenarios.

The estimated decay components are

	HH	VV	VH	HV
LOS	-1.0	-1.3	-1.7	-1.6
NLOS	-2.4	-2.2	-2.6	-2.6

As expected, decay components are much higher for the NLOS case than for the LOS case. We also see that there is a difference in the decay exponent n between the co-polarized and the cross-polarized components. As a consequence, the XPD increases with increasing distance. We find a small difference between the decay exponents of VV and HH components, but the values are quite sensitive to large scale fading in the measurements.

Comparisons with the results of [12] show that most of the general trends are similar. However, while [12] found that the VV exponent in the LOS case is smaller than the HH exponent, we find the reverse. Also, our measurement results indicate larger differences in the decay exponents of the different polarization components than [12]. We attribute those differences to the somewhat different environment (building materials) in the scenarios. As opposed to [12], the power decay of the cross- and co-polar

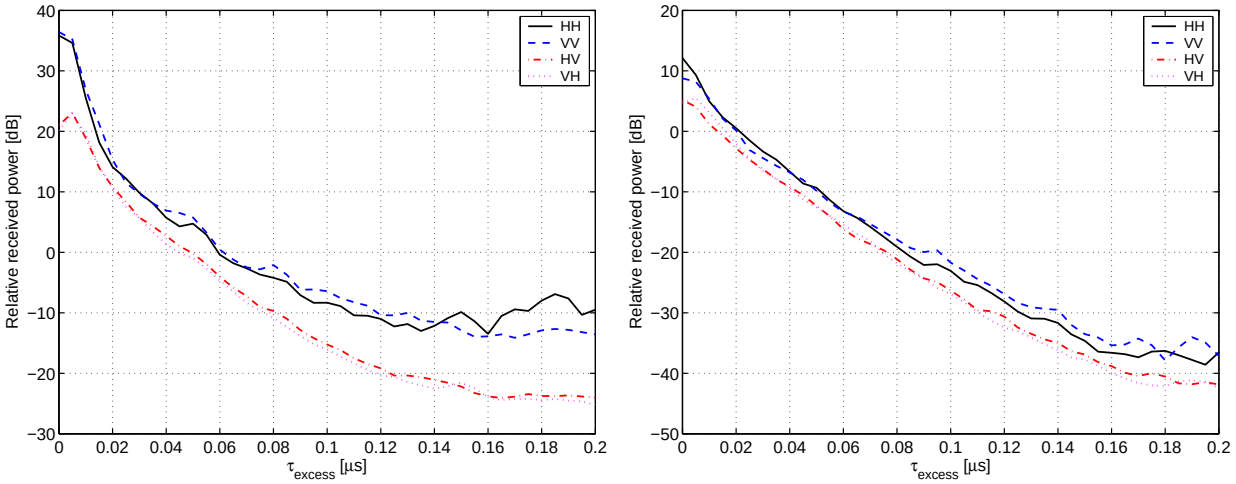

(a) an office LOS scenario

(b) an office NLOS scenario

Fig. 4. Power of the different polarization components as a function of delay

components can best be described by a power law. The XPD as a function of distance can be modeled as

$$\text{XPD}(d)|_{dB} = \text{XPD}_{d_0=1m} + n_1 \cdot 10\log_{10}(\frac{d}{d_0})$$

where $2 \leq d \leq 50$ is the distance in meters and the constants are given by the measurements as

	$\text{XPD}_{d_0=1m}$ (dB)	n_1
LOS	7.9	0.55
NLOS	2.6	0.29

We also analyzed the power of the components as a function of their delay. Fig. 4(a) shows the results in the LOS corridor. We find that both for the co-polarized and the cross-polarized components, the power delay profile decays approximately exponentially. The decay exponents are different for the co- and cross-polarized components, with the cross-polarized components decaying faster; thus, the XPD increases with the delay of the multipath components. This is a noteworthy contrast to the assumptions of the 3GPP model. However, it is also important to note that for very small delays (LOS component), the cross-polarized components are small (compared to the pure exponential law), so that the XPD at this small delay is high. Fig. 4(b) shows the results in the office NLOS environment. The conclusions are very similar.

Based on the measurements we propose the following model for the XPD as a function of the delay:

$$\text{XPD}(\tau)|_{dB} = (\text{XPD}_{HI} - \text{XPD}_{LO})\delta(\tau) + \text{XPD}_{LO} + n_2\tau,$$

where $0 \leq \tau \leq 0.2\mu s$ is the excess delay and $\delta(\tau)$ is the delta function. XPD_{HI} and XPD_{LO} are the highest and lowest measured values of XPD respectively and are given by

	XPD_{HI} (dB)	XPD_{LO} (dB)	n_2 (μs^{-1})
LOS	15.5	1.9	60
NLOS	5.9	2.1	16

IV. Spatial Correlation Properties

It is now well known that MIMO mutual information often degrades in the presence of spatial correlation. However, we also note that correlation does not always reduce capacity, as shown in a paper by [24], but for many commonly used correlation models, such as the Kronecker model, it does have this negative

effect. In order to investigate this behavior, we study the spatial correlation of the composite channel in this Section. The correlation can be expressed as a weighted sum of the constituent 2D and 3D components. Under some special conditions, analytic expressions for the constituent 2D and 3D components can be derived.

A. Spatial correlation of the 2D component

The SCM model [5] proposes distributions for the random angles and phases which define the channel coefficient. These distributions do not result in a closed form expression for the spatial correlation. In [25], a new co-polarized MIMO channel model was introduced which extends the work of Abdi and Kaveh [6] by allowing varying degrees of correlation between AoAs and AoDs. The parameters which allow this variation in correlation are κ_{BS} and κ_{MS} which are inverse angle spread (in radians) parameters similar to those in [6]. This model spans the full range of possibilities from perfect correlation between AoA and AoD (as in one-ring models) and zero correlation (as in Kronecker and SCM models [5]). In addition it leads to closed form expressions for spatial correlation. For these reasons, this model is used for the 2D component throughout this paper.

Below, we describe the spatial correlation which results from extending the model in [25], [26] to the cross-polarized case. We show that the resulting correlation has a sum-Kronecker structure (i.e, it consists of sums of Kronecker products). The following notation is used to label the antennas, which we assume are pairs of co-located cross-polarized (slant polarized) antennas. The particular antenna in the pair, s or u, is labeled by the superscript p, q in BS_s^p, MS_u^q with p and q equal to 1 or 2 representing the left or right antenna of the slant polarized antenna pair. The base station antenna p of the pair s has a slant offset angle α_p. Likewise the mobile station antenna q of the pair u has a slant offset angle α_q .

We start with the expression for the cross polarized channel coefficient (32) given in the Appendix. This is substituted into the expectation shown in (10). The resulting $\rho_{su,s'u'}^{pq,p'q'}$ terms are the elements of the 2D correlation matrix (15). In order to evaluate the expectation defining $\rho_{su,s'u'}^{pq,p'q'}$ we assume a von-Mises distribution for AoA's and AoD's. In turn, this involves evaluating double integrals due to the double summations in (32). One of the integrals has an integrand of the form $\exp\{\kappa_{BS}\Delta\sin(\theta_{i,AoA})\sin(\theta_{i,AoD}^k)\}$. We approximate this integrand by a one or two term series expansion, $\exp\{\kappa_{BS}\Delta\sin(\theta_{i,AoA})\sin(\theta_{i,AoD}^k)\} \approx 1+\kappa_{BS}\Delta\sin(\theta_{i,AoA})\sin(\theta_{i,AoD}^k)$. Taking only the unity term is denoted the "zeroth-order approximation"; taking both terms is the "first order approximation". Below, we only show results for the zeroth order approximation.

Key steps and assumptions for the derivation are shown in the Appendix, with further details available in [27]. This analysis shows that for the zeroth order approximation, we can express $\mathbf{R}^{2D}$ as a sum of four terms due to the polarization paths (VV, VH, HV, HH), where each term is a Kronecker product of four terms as shown in (15) below. We call this the sum-Kronecker channel. The resulting correlation is given by

$$\begin{aligned}\rho_{su,s'u'}^{pq,p'q'} = E[(h_{su}^{pq})(h_{s'u'}^{p'q'})^\dagger] = &\begin{bmatrix}\cos(\alpha_p)\cos(\alpha_{p'})r_{ss'}^v \\ \sin(\alpha_p)\sin(\alpha_{p'})r_{ss'}^h\end{bmatrix}^T \\ &\times \begin{bmatrix}\bar{r}^{vv} & \bar{r}^{vh} \\ \bar{r}^{hv} & \bar{r}^{hh}\end{bmatrix}\begin{bmatrix}\cos(\alpha_q)\cos(\alpha_{q'})r_{uu'}^v \\ \sin(\alpha_q)\sin(\alpha_{q'})r_{uu'}^h\end{bmatrix}\end{aligned} \tag{10}$$

The coefficients, $\bar{r}^{xy}$ are affected by the mean value and the variance of the inverse XPD and are defined by

$$\begin{bmatrix}\bar{r}^{vv} & \bar{r}^{vh} \\ \bar{r}^{hv} & \bar{r}^{hh}\end{bmatrix} = E\begin{bmatrix}1 & r_1 \\ r_2 & 1\end{bmatrix} \tag{11}$$

In order to evaluate the integrals defining $r^{v/h}_{ss'/uu'}$, we use the results below [3.937, p488, [28]]

$$\begin{aligned} F_s(p,q,a,b,m) &= \int_0^{2\pi} exp(p\cos x + q\sin x)\sin(a\cos x + b\sin x - mx)dx \\ F_c(p,q,a,b,m) &= \int_0^{2\pi} exp(p\cos x + q\sin x)\cos(a\cos x + b\sin x - mx)dx \end{aligned} \tag{12}$$

noting that [28] gives closed form expressions for both $F_s(.)$ and $F_c(.)$. With this notation, the remaining terms in (10) are given by

$$\begin{aligned} r^v_{ss'} &= \frac{I_0(\sqrt{p^2_{ss'}+q^2_{ss'}})}{I_0(\kappa_{BS})} \\ r^h_{ss'} &= \frac{1}{4\pi I_0(\kappa_{BS})} \times \{F_c(p_{ss'},q_{ss'},0,0,0)+ \\ &\quad \cos(2\phi_{BS})F_c(p_{ss'},q_{ss'},0,0,2) - \sin(2\phi_{BS})F_s(p_{ss'},q_{ss'},0,0,2)\} \\ r^v_{uu'} &= \frac{I_0(\sqrt{p^2_{uu'}+q^2_{uu'}})}{I_0(\kappa_{MS})} \\ r^h_{uu'} &= \frac{1}{4\pi I_0(\kappa_{MS})} \times \{F_c(p_{uu'},q_{uu'},0,0,0)+ \\ &\quad \cos(2\phi_{MS})F_c(p_{uu'},q_{uu'},0,0,2) - \sin(2\phi_{MS})F_s(p_{uu'},q_{uu'},0,0,2)\} \end{aligned} \tag{13}$$

where

$$\begin{aligned} &p_{ss'} = \kappa_{BS} + j2\pi d_{ss'}\sin(\phi_{BS})/\lambda \\ &q_{ss'} = -j2\pi d_{ss'}\cos(\phi_{BS})/\lambda \\ &p_{uu'} = \kappa_{MS}\cos(\bar{\phi}_{AoA}) + j2\pi d_{uu'}\sin(\phi_{MS})/\lambda \\ &q_{uu'} = \kappa_{MS}\sin(\bar{\phi}_{AoA}) - j2\pi d_{uu'}\cos(\phi_{MS})/\lambda \\ &d_{ss'} = \text{distance between BS antenna pair s and } s' \text{ in } \lambda \\ &d_{uu'} = \text{distance between MS antenna pair u and } u' \text{ in } \lambda \\ &\bar{\phi}_{AoA} = \text{mean angle of arrival} \\ &I_0 = \text{zeroth-order modified Bessel function of the first kind} \end{aligned} \tag{14}$$

For normal antenna configurations with symmetric antenna pairs and BS/MS slant offset angle α_{BS}/α_{MS}, from (10) the channel correlation matrix $\mathbf{R}^{2D}$ can be expressed as

$$\begin{aligned} \mathbf{R}^{2D} = E\left[vec(\mathbf{H}^{2D})vec(\mathbf{H}^{2D})^\dagger\right] = \sum_{x,y=v,h} \bar{r}^{xy} \times \\ \left((\mathbf{R}^x_{BS} \bigotimes \mathbf{\Omega}^x_{BS}) \bigotimes (\mathbf{R}^y_{MS} \bigotimes \mathbf{\Omega}^y_{MS})\right) \end{aligned} \tag{15}$$

where each element of $\mathbf{R}^{2D}$ comes from (10) and can be reorganized in the sum-Kronecker form shown in (15). $\mathbf{R}^{v/h}_{BS/MS}$ is the matrix form of (13) and

$$\begin{aligned} \mathbf{\Omega}^v_{BS/MS} &= \cos^2(\alpha_{BS/MS}) \begin{bmatrix} 1 & 1 \\ 1 & 1 \end{bmatrix} \\ \mathbf{\Omega}^h_{BS/MS} &= \sin^2(\alpha_{BS/MS}) \begin{bmatrix} 1 & -1 \\ -1 & 1 \end{bmatrix} \end{aligned} \tag{16}$$

B. Spatial correlation of the 3D component

Here we describe the correlation properties of h^{3D}. For simplicity, we focus on ideal dipole antennas, as they carry many of the properties of most antennas and we also assume that the number of scatterers is sufficiently large so that we may replace the sums in (7) with integrals. The spatial correlations of two pairs of antennas at transmitter and receiver ends take the following Kronecker product form assuming $r_1 = r_2 = 1$. This is justifiable as in the 3D case the angles of arrival and departure are independent due to significant local scattering.

$$\mathbf{R}^{3D} = E\left[vec(\mathbf{H}^{3D})vec(\mathbf{H}^{3D})^{\dagger}\right] = \mathbf{R}^{3D}_{BS} \otimes \mathbf{R}^{3D}_{MS} \tag{17}$$

$\mathbf{R}^{3D}_{BS}$ and $\mathbf{R}^{3D}_{MS}$ are the base-station and mobile correlation matrices. The elements of $\mathbf{R}^{3D}_{BS}$ are given by

$$\begin{aligned} R^{3D}_{nn',BS} &= \int_0^{2\pi} d(\phi_{AoD})P(\phi_{AoD})e^{ikd_{nn'}\cos\phi_{AoD}} \\ &\quad \left[\cos\left(\alpha_n - \alpha_{n'}\right) - \sin\alpha_n \sin\alpha_{n'} \sin^2\phi_{AoD}\right] \end{aligned} \tag{18}$$

with $P(\phi_{AoD})$ the power angle spectrum at the base station [5], ϕ_{AoD} the azimuth angle measured from the perpendicular of the antenna array and $k = |\mathbf{k}|$. The indices of the antennas n, n' are taken over all antennas in the array, including colocated and non-colocated antennas. α_n, $\alpha_{n'}$ are the elevation tilts of the antennas n, n' measured from the z-axis and $d_{nn'}$ is the spatial distance between BS antennas n, n'. This form of the correlation is identical to those derived from (3) using $r = 1$ [5]. The correlation at the mobile side is more interesting and takes the form

$$\begin{aligned} R^{3D}_{mm',MS} &= \int d\Omega_{\mathbf{k}} e^{i\mathbf{k}\mathbf{d}_{mm'}} \left[\mathbf{p}^{\dagger}_m \mathbf{p}_{m'} - (\mathbf{p}^{\dagger}_m \hat{\mathbf{k}})(\hat{\mathbf{k}}^{\dagger}\mathbf{p}'_m)\right] \\ &= \mathbf{p}^{\dagger}_m \mathbf{p}_{m'} f_0(kd_{mm'}) \\ &+ \left[\frac{1}{3}\mathbf{p}^{\dagger}_m \mathbf{p}_{m'} - (\mathbf{p}^{\dagger}_m \hat{\mathbf{d}}_{mm'})(\hat{\mathbf{d}}^{\dagger}_{mm'}\mathbf{p}_{m'})\right] f_1(kd_{mm'}) \end{aligned} \tag{19}$$

In the above equation $\hat{\mathbf{k}}$ is the unit vector in the direction of $\mathbf{k}$. Similarly, $\hat{\mathbf{d}}_{mm'}$ is the unit vector along the direction of $\mathbf{d}_{mm'}$, which is the vector between the locations of antennas m, m'. $\mathbf{p}_m$, $\mathbf{p}_{m'}$ are the (unit) polarization vectors of the MS antennas m, m'. For dipole antennas, these are along the axis of the antenna. Finally, $f_0(x)$ and $f_1(x)$ are functions given by

$$\begin{aligned} f_0(x) &= \frac{\sin x}{x} \\ f_1(x) &= \frac{3}{2}\left[\frac{\sin x}{x} - 3\left(\frac{\sin x}{x^3} - \frac{\cos x}{x^2}\right)\right] \end{aligned} \tag{20}$$

The form of the correlations at the mobile have two interesting implications. First, since $f_0(0) = 1$ and $f_1(0) = 0$, for co-located antennas, we can have 3 mutually independent antennas with polarizations orthogonal to each other [29]. Second, one can form an uncorrelated uniform linear array (co-polarized) with minimum distance $\lambda/2$ only if the antennas are tilted in a special way. Otherwise, the term proportional to f_1 in (19) will not vanish. The simplest way to make eliminate this term is by tilting the antennas by 54.73^o with respect to the line connecting them [7].

C. Overall correlation

The overall correlation matrix for the MIMO system is given by a weighted sum as follows:

$$\mathbf{R} = \frac{1}{1+g}\mathbf{R}^{2D} + \frac{g}{1+g}\mathbf{R}^{3D} \tag{21}$$

Fig. 5 shows the spatial correlation at the MS for the 2D, 3D and composite components. Analytical results from (15), (19) and (21) matched simulations of the SCM model extremely well. In these results $\phi_{BS} = \phi_{MS} = 0^{\circ}$ and other parameters can be found in Table I.

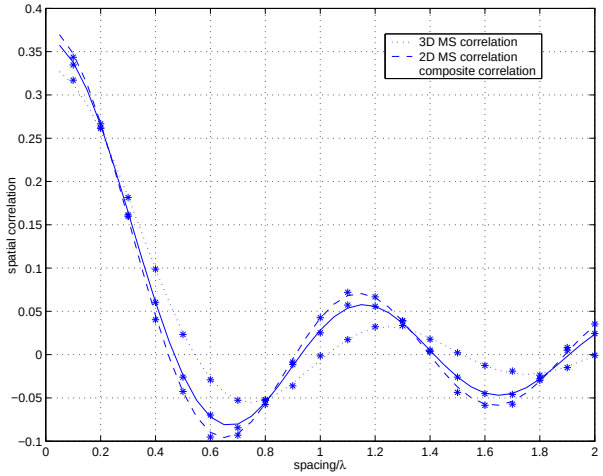

Fig. 5. Spatial correlation at the MS vs spacing

Parameter	Value	Parameter	Value
N	6	M	20
SNR	18dB	ϕ_{MS}	0°
ϕ_{BS}	0°	PAS in Kronecker	Von Mises
PAS in SCM	Laplacian	$f_D = \|v\|/\lambda$	0.04
θ_v	0°	$\bar{\theta}_{AoA}$	0°
κ_{BS}	100	κ_{MS}	0.5

TABLE I
PARAMETERS FOR SCM SIMULATIONS AND ANALYSIS

V. Results and Discussions

The ergodic mutual information (MI) is given by the classic equation [30]

$$\mathcal{I} \;=\; E\left[\log_2 \det\left(\mathbf{I}_{n_{MS}} + \frac{SNR}{n_{BS}}\mathbf{H}\mathbf{H}^\dagger\right)\right] \tag{22}$$

where the expectation is over the realizations of the channel matrix $\mathbf{H}$ and the BS is the transmitter. It is assumed that channel state information is only known at the receiver. The mean MI (MMI) is the average value of MI over different orientations of BS and MS. We assume unit antenna gain at both the BS and MS. Both the SCM model (9) and the sum-Kronecker correlation structure (21) with Rayleigh fading are used to calculate MI. Important parameter values and distributional assumptions used in the numerical results can be found in Table I. Where parameter values are not given, we have used the suburban macro environment parameters in [5]. The values of κ_{BS}, κ_{MS} were chosen to approximate the SCM model.

A. Impact of slant angle on correlation for different XPD values

In order to study the relationship between the optimal slant offset angle (with maximal MI) and other channel parameters we consider a (2,2) cross-polarized MIMO system with zero 3D component and the sum-Kronecker structure (15). Note that at high SNR, the log-determinant in (22) is almost linear so that maximizing MI over slant offset angle α is similar to maximizing $\bar{\zeta} = E[\det(\mathbf{I}_2 + \frac{SNR}{2}\mathbf{H}\mathbf{H}^\dagger)]$. Also at low SNR, the first order approximation $\mathcal{I} \approx \bar{\zeta}$ is accurate since the variance of the determinant in (22) is small. Hence, for these special cases, we can focus on $\bar{\zeta}$ rather than $\mathcal{I}$. Here, some routine analysis

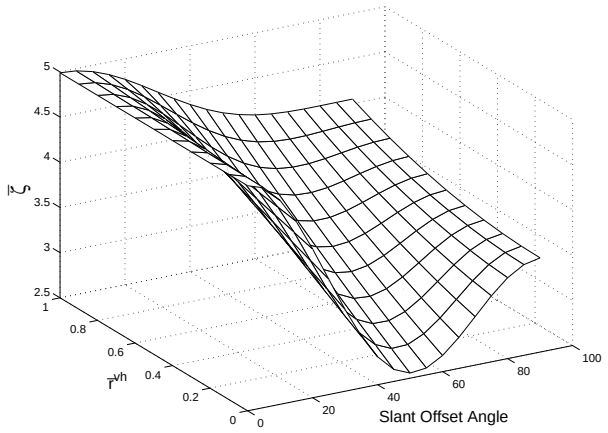

Fig. 6. $\bar{\zeta}$ vs $\bar{r}^{vh}$ and the slant offset angle for low SNR case(SNR=3dB)

shows that $\bar{\zeta}$ can be expressed as

$$\begin{aligned}\bar{\zeta} = 1 + SNR\Bigg\{ & 2\cos^4\alpha + \left(1 + \frac{I_2(\kappa_{BS})}{I_0(\kappa_{BS})}\right)\bar{r}^{vh}\sin^2\alpha\cos^2\alpha \\ & + \left(1 + \frac{I_2(\kappa_{MS})}{I_0(\kappa_{MS})}\right)\bar{r}^{hv}\sin^2\alpha\cos^2\alpha + \frac{1}{2}\left(1 + \frac{I_2(\kappa_{BS})}{I_0(\kappa_{BS})}\right)\left(1 + \frac{I_2(\kappa_{MS})}{I_0(\kappa_{MS})}\right)\sin^4\alpha\Bigg\} \\ & + SNR^2\Bigg\{\left(1 + \frac{I_2(\kappa_{BS})}{I_0(\kappa_{BS})}\right)\left(1 + \frac{I_2(\kappa_{MS})}{I_0(\kappa_{MS})}\right) \times \left(\bar{r}^{vh}\bar{r}^{hv} + 1\right)\sin^4(2\alpha)/16\Bigg\}\end{aligned} \tag{23}$$

Equation (23) reveals several important conclusions:

- At low SNR, the second term is the major factor. Using $0 < \bar{r}^{vh} = \bar{r}^{hv} < 1$ and Bessel function approximations for large arguments (κ_{BS}) and small arguments (κ_{MS}), close inspection of (23) shows that the optimal slant offset angle is always 0° implying perfect correlation. Note that Fig. 6 verifies this remark numerically for $\kappa_{BS} = 500$ and $\kappa_{MS} = 0.5$. An optimal slant offset angle of 0° means that antenna pairs do not have slant offset angles and the cross-polarized system reduces to the co-polarized system.
- When the SNR is large, the third term will dominate and the optimal slant offset angle is always 45° irrespective of any other parameters such as $\kappa_{BS}, \kappa_{MS}, XPD$. Again, this makes sense since the slant angle of 45° reduces correlation and at large SNR, uncorrelated channels are better since we can transmit multiple streams.

Next we simulate a larger (8,8) cross-polarized MIMO system with $\bar{\phi}_{AoA} = 0$, $\phi_{BS} = \phi_{MS} = 0$, $\kappa_{BS} = 100$ or 500, $\kappa_{MS} = 0.5$, $d_{ss'} = \lambda$, $d_{uu'} = 0.5\lambda$. The XPD's are independently generated by $r_1 = r_2 = 10^{(-4.5+5.5\eta(0,1))/10}$ or $r_1 = r_2 = 10^{(-8.5+5.5\eta(0,1))/10}$ where $\eta(0,1)$ is a standard normal variable [5]. These equations enable us to vary the XPD and study the impact on MI. Varying offset angles in both the BS and the MS, we obtain the results in Fig. 7. This shows that the cross-polarized MIMO system can not perform better than the co-polarized system (with 0° slant offset angle) when the power is small (shown in Fig. 7(a)). Whereas the optimal offset angle will vary from 35° to 45° at large SNR and it will be closer to 45° when the power is increased (shown in Fig. 7(b)).

B. Impact of array width on co-polarized and cross-polarized correlation

The slant offset angle used here is 45° in the BS and the MS and the MI is spatially averaged over 10,000 drops with uniformly distributed orientations of BS and MS. Fig. 8 shows MMI comparisons among different MIMO systems using the composite SCM channel (9) and the sum-Kronecker correlation model

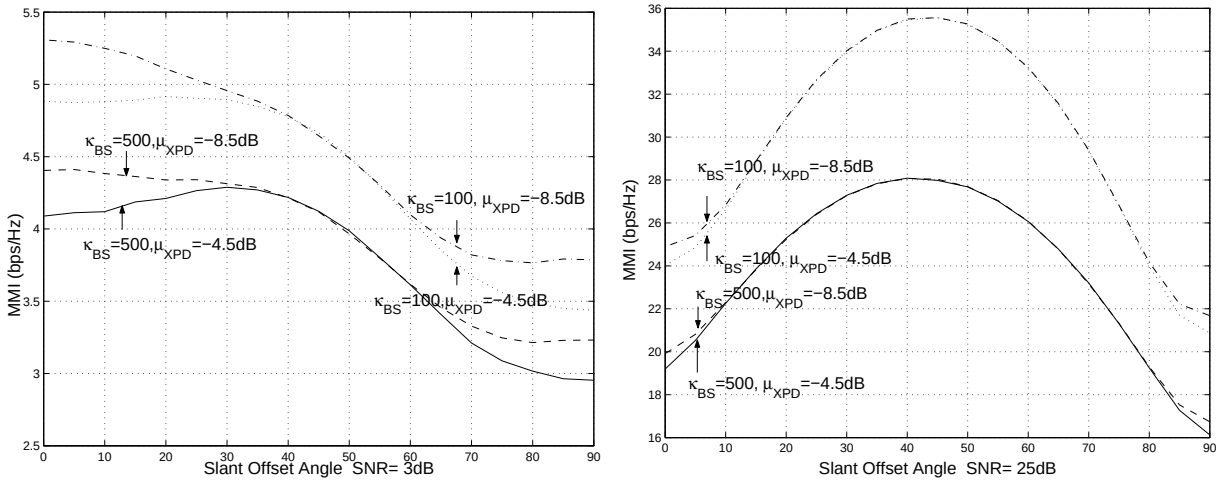

(a) SNR = 3dB (b) SNR = 25dB

Fig. 7. MMI vs slant offset angle for various SNR values

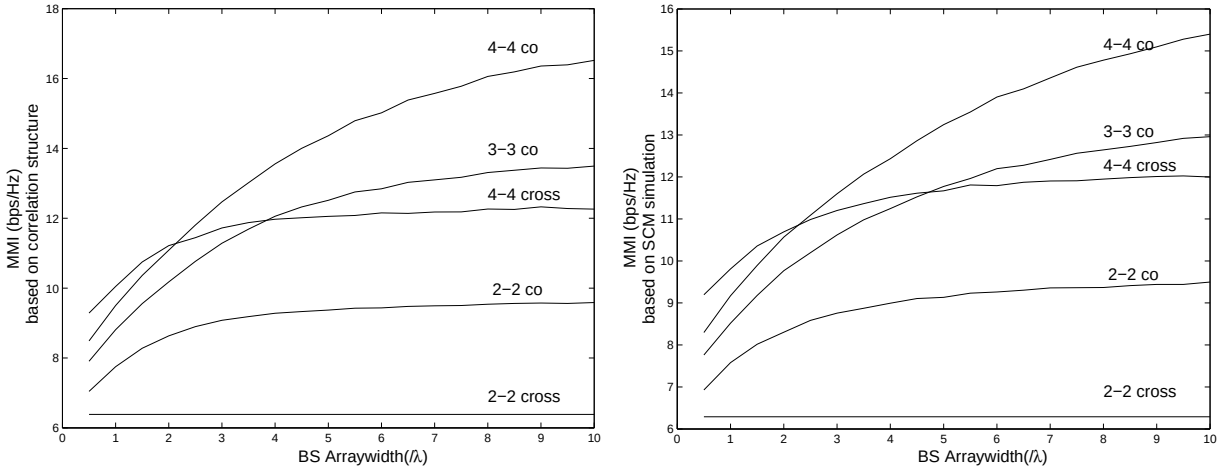

(a) Correlation model (b) SCM model

Fig. 8. MMI vs BS array width for co- and cross- polarized systems (SNR=18dB)

(21). The Monte Carlo method is used to generate the channel coefficients for the correlation model. Both models perform similarly and the benefits and drawbacks of cross-polarized MIMO are clear. At very small spacings the cross-polarized system outperforms the co-polarized system. This occurs for BS antenna spacings less than about 2.2 wavelengths for (4-4) systems. The (4-4) cross-polarized system is worse than the (3-3) co-polarized system when the BS spacing is larger than 4 wavelengths. This is reasonable since when the spacing is increased, the correlation between BS antennas always decreases in a co-polarized MIMO system. However, half of the antennas are still strongly correlated in the cross-polarized MIMO system. For a given spacing, the MIMO system benefits from increased numbers of antenna elements but is impaired by higher correlation.

C. Large system MI analysis

It would be useful to have an analytic expression for the mutual information for the channels discussed thus far. For the case of Gaussian channels with Kronecker product correlated channels, the statistics of the mutual information are well understood, since exact closed form expressions for the moment generating function exist for both semi-correlated [31], [32] and fully correlated [33], [34], [35] channels. However, these methods cannot be generalized to non-Kronecker product correlations. Therefore, to make analytic

progress, one needs to employ asymptotic methods. In [36] such methods were used to calculate the first few moments of the distribution of the mutual information for non-Kronecker product correlations in the limit of large antenna numbers. Fortunately, these methods are accurate also for a few (2-3) antennas [37].

In this section we apply these methods to calculate the ergodic mutual information of a (n_t, n_r) MIMO link for the composite cross-polarized channels developed here. For the case of outdoor propagation one can simply disregard g by setting it to zero. The correlations of the composite channel matrix may be written as

$$E\left[\mathbf{H}_{i\alpha}\mathbf{H}^*_{j\beta}\right] = \frac{P}{(1+g)n_t}\begin{bmatrix} R^{2D,v}_{BS,\alpha\beta} \\ R^{2D,h}_{BS,\alpha\beta}\end{bmatrix}^T \mathbf{M}\begin{bmatrix} R^{2D,v}_{MS,ij} \\ R^{2D,h}_{MS,ij}\end{bmatrix} + \frac{gP}{(1+g)n_t} R^{3D}_{BS,\alpha\beta} R^{3D}_{MS,ij} \tag{24}$$

where P is the signal to noise ratio of each path, g is the 3-dimensional mixing parameter, $R^{3D}_{BS,ij}$ are the correlations between antennas i, j at the base for the 3-dimensional propagation (with a corresponding expression for the mobile), $R^{2D,v}_{BS,ij}$ are the correlations of the vertical polarization (and similarly for the horizontal polarization and the mobile) and $\mathbf{M}$ is the mixing matrix

$$\mathbf{M} = \begin{bmatrix} 1 & r \\ r & 1\end{bmatrix} \tag{25}$$

where we assume $r = E[r_1] = E[r_2]$.

Using the replica approach and saddle-point analysis, the ergodic mutual information can be written as:

$$\mathcal{I} = \log\det\left(\mathbf{I}_{n_t} + \tilde{\mathbf{T}}\right) + \log\det\left(\mathbf{I}_{n_r} + \tilde{\mathbf{R}}\right) - n_t\sum_{a=1}^{3} x_a y_a \tag{26}$$

where the matrices $\tilde{\mathbf{T}}$, $\tilde{\mathbf{R}}$ are given by

$$\begin{aligned} \tilde{\mathbf{T}} &= \frac{P}{1+g}\left[(y_1 + r y_2)\,\mathbf{R}^{2D,v}_{BS} + (r y_1 + y_2)\,\mathbf{R}^{2D,h}_{BS}\right] + \frac{gP}{1+g} y_3 \mathbf{R}^{3D}_{BS} \\ \tilde{\mathbf{R}} &= x_1\mathbf{R}^{2D,v}_{MS} + x_2\mathbf{R}^{2D,h}_{MS} + x_3\mathbf{R}^{3D}_{MS} \end{aligned} \tag{27}$$

with the scalars x_a, y_a, for $a = 1, 2, 3$ given by

$$\begin{aligned} x_1 &= \frac{P}{(1+g)n_t} tr\left[\left(\mathbf{R}^{2D,v}_{BS} + r\mathbf{R}^{2D,h}_{BS}\right)\left(\mathbf{I}_{n_t} + \tilde{\mathbf{T}}\right)^{-1}\right] \\ x_2 &= \frac{P}{(1+g)n_t} tr\left[\left(\mathbf{R}^{2D,h}_{BS} + r\mathbf{R}^{2D,v}_{BS}\right)\left(\mathbf{I}_{n_t} + \tilde{\mathbf{T}}\right)^{-1}\right] \\ x_3 &= \frac{gP}{(1+g)n_t} tr\left[\mathbf{R}^{3D}_{BS}\left(\mathbf{I}_{n_t} + \tilde{\mathbf{T}}\right)^{-1}\right] \end{aligned} \tag{28}$$

$$\begin{aligned} y_1 &= \frac{1}{n_t} tr\left[\mathbf{R}^{2D,v}_{MS}\left(\mathbf{I}_{n_t} + \tilde{\mathbf{R}}\right)^{-1}\right] \\ y_2 &= \frac{1}{n_t} tr\left[\mathbf{R}^{2D,h}_{MS}\left(\mathbf{I}_{n_t} + \tilde{\mathbf{R}}\right)^{-1}\right] \\ y_3 &= \frac{1}{n_t} tr\left[\mathbf{R}^{3D}_{MS}\left(\mathbf{I}_{n_t} + \tilde{\mathbf{R}}\right)^{-1}\right] \end{aligned} \tag{29}$$

Results in Fig. 9 show how closely the large sample results follow the simulation for an (8-8) system. The sensitivity of MI to the g factor is also shown in Fig. 9. Two cases are considered: $\kappa_{MS} = 500$ corresponds to the mobile receiving signals with low angle spread and $\kappa_{MS} = 0.5$ corresponds to signals arriving uniformly from all directions. The abscissa is drawn for g values corresponding to the 2D component alone to the case where the 3D component dominates. The MI is very sensitive to the value of the g

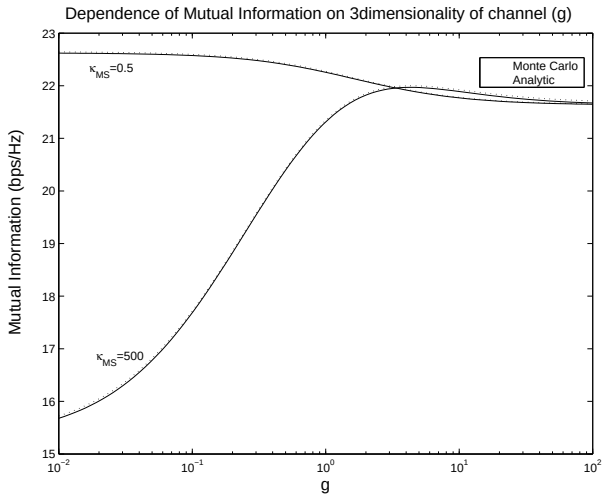

Fig. 9. MI vs g with 4 pairs of cross-polarized antennas at both ends (SNR=18dB, $\phi_{BS} = \phi_{MS} = 0^\circ$)

parameter, especially for the low angle spread case. The low angle spread case may arise when the mobile receives signals from a narrow range due to building construction (i.e., the presence of windows). When the angle spread is small, the 3D component results in a substantial overall increase of the MI with increasing g.

D. Temporal dependence of XPD and impact on system capacity

In this Section, we analyze the impact that the temporal dependence of the XPD has on the capacity of a polarization-based MIMO-CDMA system. In order to characterize the capacity of a MIMO-CDMA system, we investigate the capacity C_{mf} of the matched-filter bound, i.e., the capacity that would be achievable if no intersymbol interference occurs. For a system with a high spreading factor N_{sp} and sufficiently low data rate, the capacity of each single user is given by $C_{\text{mf}}/N_{\text{sp}}$. We show that for such a system, operating in the 3GPP channel model [5], the impact of the delay dependence of the XPD on the system capacity is negligible. Further simulations (not shown here) show that this result also holds for the 3D model, and for systems that use OFDM instead of CDMA.

C_{mf} can be computed in a straightforward way: each Rake finger collecting energy from one antenna element can be considered as a "virtual" antenna, so that a $n_{MS} \times n_{BS}$ polarization-based MIMO system with N_{R} Rake fingers corresponds to a virtual $n_{MS}N_{\text{R}} \times n_{BS}$ system. The entries in the channel matrix are obtained directly from the 3GPP model or from our new model, where each path leads to a $n_{MS} \times n_{BS}$ submatrix; the submatrices are stacked horizontally into a total matrix $\mathbf{H}$. For a WSSUS channel, the entries of one submatrix are statistically independent of the other submatrices. Note that the power carried by each of the submatrices (i.e., its Frobenius norm) is proportional to the power delay profile at delay τ_n. The capacity of this "equivalent" or "virtual" system can be computed by the classical capacity equation (22).

Both due to the different powers collected by the different Rake taps, and because of the cross-polarization discrimination, the entries in the matrix $\mathbf{H}$ are non-identically distributed (i.e., all of the entries have a complex Gaussian distribution, but with different variances). Fig. 10 shows the capacity of a system with $n_{BS} = n_{MS} = 2$ where TX and RX transmit and receive, respectively, on both the horizontal and vertical polarizations. The system operates in a 3GPP urban channel. Fig. 10(a) shows the capacity when using only a single Rake finger (always matched to the first path), while Fig. 10(b) shows the result when 6 Rake fingers are used (i.e., all energy from the paths can be collected). Similar mean channel capacity is shown compared with Fig. 8; any small differences between them may come from different assumptions forthe XPD values. Note that in the 3GPP urban model, the XPD decreases with the

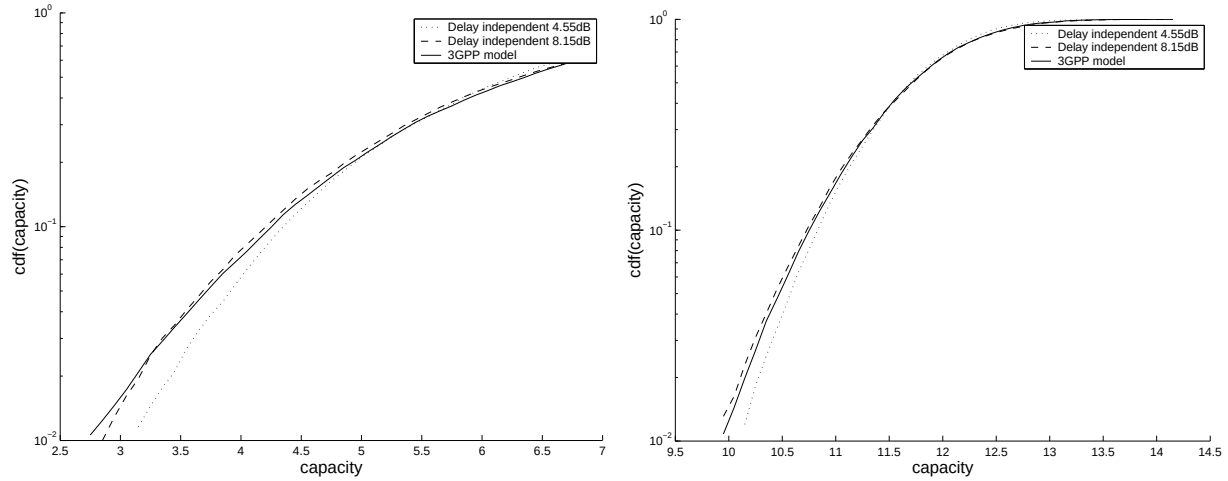

(a) a single Rake finger (b) six Rake fingers

Fig. 10. Capacity of a polarization-based 2*2 MIMO system with Rake receiver (matched filter bound) with 1 finger and 6 fingers. The channel XPD depends on the delay according to the 3GPP model (solid), delay independent 4.55 dB XPD (dotted), delay-independent 8.15 dB XPD(dashed) (SNR=18dB).

power of the multipath components (and thus, with their delay). The results for this case are compared to the cases where the XPD is independent of the delay; the value in that case is chosen in such a way that the *narrowband* XPD is the same in both cases. We see that the difference between the two cases is rather minor. However, it is noteworthy that for the case of a single Rake finger, the constant-XPD is slightly better than the delay-dependent XPD, while for the full Rake receiver (6 fingers) the results are virtually identical. We also note that a difference occurs only for the outage probability at low outage levels, while the mean capacity is indistinguishable.

VI. Conclusions

4G systems are expected to support data rates of the order of 100 Mbps in the outdoor environment and 1 Gbps in the indoor/stationary environment. In order to support such large pay loads, MIMO based receiver techniques are receiving considerable interest. Cross-polarized antennas may be used in 4G wireless systems using MIMO receivers. An understanding of multi-antenna systems and their channels will help us to develop efficient methods of interference mitigation in the presence of multiple users.

In this paper we present a novel approach to describe a MIMO cross polarized channel. This consists of defining a composite channel coefficient that is a scaled sum of 2D and 3D components. The 3D component is new and aims to model indoor and in vehicle situations. The 2D component of the model is based on a sum-Kronecker structure of the spatial correlation. This approach for the 2D component is quite general as it is able to generate both the sum-Kronecker and the simple Kronecker structures. The 2D and 3D components are scaled via a g parameter to form the composite channel. The composite channel is then used to derive a closed form expression for the ergodic mutual information for large systems. The accuracy of the closed form expression is verified by simulation.

One parameter that influences the gain of cross-polarized channels is XPD. We present a comprehensive model that shows the dependence of XPD on distance and the delay profile. We determine the parameters of the model from field measurements and show their impact on capacity.

The mean or ergodic mutual information for the composite channel is very sensitive to the value of the g parameter especially when the mobile station is in an environment of low angle spread. This is feasible as most of the energy reaching the mobile may be coming from a certain range of angles due to building construction (e.g. the presence of windows) rather than uniformly in all directions. Our simulations also

provide insight into various practical issues e.g. how the mean mutual information for a cross-polarized system is influenced by antenna spacings, angle spreads, XPD, antenna slant offset angles etc.

We believe the studies reported here will be of value in system design studies of 4G wireless systems that use MIMO techniques.

ACKNOWLEDGEMENTS

The authors would like to thank Johan Kåredal, Lund University, for his assistance with respect to the measurements.

REFERENCES

[1] S. Kozono, T. Suruhara and M. Sakamoto, "Base station ploarization diversity reception for mobile radio," *IEEE Trans. on Vehi. Tech.*, vol. 33, no. 4, pp. 301–306, Nov. 1984.
[2] R.G. Vaughan, "Polarisation diversity in mobile communications," *IEEE Trans. on Vehi. Tech.*, vol. 39, no. 3, pp. 177–185, June 1990.
[3] T. Taga, "Analysis for the mean effective gain of mobile antennas in land mobile radio environments," *IEEE Trans. on Vehi. Tech.*, vol. 39, no. 2, pp. 117–131, May 1990.
[4] K. Kalliola, K. Sulonen, H. Latinen, O. Kivekas, J. Krogerus and P. Vainikainen, "Angular power distribution and mean effective gain of mobile natenna in different propagation environments," *IEEE Trans. on Vehi. Tech.*, vol. 51, no. 5, pp. 823–838, Sep. 2002.
[5] "Spatial channel model for multiple input multiple output MIMO simulations," *3GPP*, vol. TR 25.996, v6.1.0, Sep. 2003.
[6] A. Abdi and M.Kaveh, "A space-time correlation model for multi-element antenna systems in mobile fading channels," *IEEE J. on Sele. Areas in Comm.*, vol. 20, no. 3, pp. 550 – 560, Apr. 2002.
[7] A.L. Moustakas, H.U. Baranger, L. Balents, A.M. Sengupta and S.H. Simon, "Communication through a diffusive medium: Coherence and capacity," *Science*, vol. 287, pp. 287–290, Jan. 2000.
[8] L. Correia, *Wireless Flexible Personalised Communications; COST 259: European Co-operation in Mobile Radio Research*. Chichester, UK: John Wiley and Sons, 2001.
[9] C. A. Balanis, *Antenna Theory: Analysis and Design*. USA: John Wiley and Sons, 1982.
[10] C. F. T. Zwick and W. Wiesbeck, "A stochastic multipath channel model including path directions for indoor environments," *IEEE J. on Sele. Areas in Comm.*, vol. 20, no. 6, pp. 1178–1192, Aug. 2002.
[11] M.B. Knudsen and G.F. Pedersen, "Spherical outdoor to indoor power spectrum model at the mobile terminal," *IEEE J. on Sele. Areas in Comm.*, vol. 20, no. 6, pp. 1156–1169, Aug. 2002.
[12] P. Kyritsi, D.C. Cox, R.A. Valenzuela, and P.W. Wolniansky, "Effect of antenna polarization on the capacity of a multiple element system in an indoor environment," *IEEE J. on Sele. Areas in Comm.*, vol. 20, no. 6, pp. 1227–1239, Aug. 2002.
[13] T.S. Rappaport and D. A. Hawbaker, "Wide-band microwave propagation parameters using circular and linear polarized antennas for indoor wireless channels," *IEEE Trans. Comm.*, vol. 40, no. 2, pp. 240–245, 1992.
[14] X. Zhao, S. Geng, L. Vuokko, J. Kivinen, and P. Vainikainen, "Polarization behaviours at 2, 5 and 60 GHz for indoor mobile communications," *Wireless Personal Comm.*, vol. 27, pp. 99–115, 2003.
[15] P. Soma, D.S. Baum, V. Erceg, R. Krishnamoorthy, and A.J. Paulraj, "Analysis and modeling of multiple-input multiple-output MIMO radio channel based on outdoor measurements conducted at 2.5 GHz for fixed BWA applications," *IEEE ICC*, vol. 1, pp. 272–276, 2002.
[16] L.C. Palma Pereira and T.A. Suedan, "An experimental evaluation of the polarization characteristics of mobile communication signals at 800 MHz," *Microwave and Optoelectronics Conference*, pp. 177–182, 2003.
[17] A. Kara and H.L. Bertoni, "Blockage/shadowing and polarization measurements at 2.45GHz for interference evaluation between bluetooth and IEEE 802.11 WLAN," *Int. Symp. Antennas and Propagation*, pp. 376–379, 2001.
[18] T. Neubauer and P.C. F Eggers, "Simultaneous characterization of polarization matrix components in pico cells," *Proc. VTC*, pp. 1361–1365, 1999, 1999.
[19] K.I. Pedersen, P.E. Mogensen and B.H. Fleury, "Dual-polarized model of outdoor propagation environments for adaptive antennas," *Proc. VTC*, no. 990-995, 1999.
[20] M. Nilsson, B. Lindmark, M. Ahlberg, M. Larsson, and C. Beckman, "Measurements of the spatio-temporal polarization characteristics of a radio channel at 1800 MHz," *Proc. VTC*, pp. 386–391, 1999.
[21] P.C.F. Eggers, J. Toftgaard , A.M. Oprea, "Antenna systems for base station diversity in urban small and micro cells," *IEEE J. on Sele. Areas in Comm.*, vol. 7, pp. 1046–1057, 1993.
[22] M. Toeltsch, J. Laurila, K. Kalliola, A. F. Molisch, P. Vainikainen, and E. Bonek, "Statistical characterization of urban spatial radio channels," *IEEE J. on Sele. Areas in Comm.*, vol. 20, pp. 539–549, 2002.
[23] J. Karedal, F. Tufvesson, and A.F. Molisch, "Measurements of polarization effects in indoor office environments," Department of Electroscience, Lund University, Tech. Rep. No. 7, ISSN 1402-8840, Feb 2005.
[24] C. Oestges and A. Paulraj, "Beneficial impact of channel correlations on MIMO capacity," *Electronics Letters*, vol. 40, no. 10, pp. 606–608, May 2004.
[25] M. Zhang, P. J. Smith and M. Shafi, "A new space time MIMO channel model," *Proc. AusCTW*, pp. 280–285, 2005.
[26] P.J. Smith and M. Shafi, "The use of cross-polarized antennas for MIMO systems," *Proc. AusCTW*, pp. 133–138, Feb. 2004.
[27] M. Zhang, "A novel spatial-temporal MIMO channel model," *M.Sc. Thesis, Dept. of ECE, University of Canterbury, Christchurch, NZ*, 2005.
[28] I.S. Gradshteyn and I.M. Ryzhik, *Table of Integral, Series, and Products*, corrected and enlarged ed. Academic Press, 1980.

[29] M. Andrews, P.P. Mitra and R. deCarvallo, "Tripling the capacity of wireless communications using electromagnetic polarization," *Nature*, vol. 406, pp. 316–318, Jan. 2001.
[30] I.E. Telatar, "Capacity of multi-antenna Gaussian channels," *European Trans. on Tele.*, vol. 10, no. 6, pp. 585–595, 1999.
[31] P.J. Smith, S. Roy and M. Shafi, "Capacity of MIMO systems with semicorrelated flat fading," *IEEE Trans. on Info. Theory*, vol. 49, no. 10, pp. 2781–2788, Oct. 2003.
[32] M. Chiani, M.Z. Win and A. Zanella, "On the capacity of spatially correlated MIMO Rayleigh-fading channels," *IEEE Trans. on Info. Theory*, vol. 49, no. 10, pp. 2363–2371, 2003.
[33] S.H. Simon and A.L. Moustakas, "Eigenvalue density of correlated random Wishart matrices," *Phys. Rev. E*, vol. 69, no. 065101, June 2004.
[34] S.H. Simon, A.L. Moustakas and L. Marinelli, "Capacity and character expansions: moment generating function and other exact results for MIMO correlated channels," *submitted for publication*, Mar. 2004.
[35] M. Kiessling and J. Speidel, "Mutual information of MIMO channels in correlated Rayleigh fading environments - a general solution," *IEEE ICC*, vol. 2, pp. 814–818, June 2004.
[36] A.L. Moustakas and S.H. Simon, "On the outage capacity of correlated multipath MIMO channels," *submitted for publication*.
[37] P.J. Smith and M. Shafi, "On a Gaussian approximation to the capacity of wireless MIMO systems," *IEEE ICC*, vol. 1, pp. 406–410, May 2002.

APPENDIX: CORRELATIONS FOR THE CROSS-POLARIZED 2D CHANNEL MODEL

When the channel correlation matrix can be represented as

$$\mathbf{R} = \mathbf{E}\left[vec(\mathbf{H})vec(\mathbf{H})^{\dagger}\right] = \sum_{k} \mathbf{R}_{BS}^{k} \bigotimes \mathbf{R}_{MS}^{k} \tag{30}$$

and $k > 1$, we refer to such a model as a "sum-Kronecker" correlation model and define the model as a "single-Kronecker" correlation model when $k = 1$. Note that in a slight abuse of notation, we use the superscript k in $\mathbf{R}_{BS}^{k}$ and $\mathbf{R}_{MS}^{k}$ to explain a sum-Kronecker channel. However $\mathbf{R}_{BS}^{x}$ and $\mathbf{R}_{BS}^{y}$ have different meanings as given in (15).

The channel coefficient matrix for the sum-Kronecker model, assuming Rayleigh fading, can be written as:

$$\mathbf{H} = \sum_{k} \left(\mathbf{R}_{MS}^{k}\right)^{1/2} \mathbf{H}_{w}^{k} \left[\left(\mathbf{R}_{BS}^{k}\right)^{1/2}\right]^{T} \tag{31}$$

where $\mathbf{H}_{w}^{k}$ is the k^{th} i.i.d random matrix with zero-mean and unit variance complex Gaussian entries. This is how we simulate the 2D channel in all cases where the new 2D or composite model is being used.

In our 2D model [25], the BS transmits signals with a narrow beamwidth Δ and the MS receives them from a large number of local scatterers surrounding the MS. We do not consider LoS in the system and only model a single ray at the MS which can be interpreted as a sum over subrays from the ith scatterer S_i. Here, each AoA (path) is not associated with one specified AoD as in one-ring models, but a cluster of AoDs (subpaths) with given power azimuth spectrum. Let g_i be the wave amplitude of the ith path defined by the arrival angle $\phi_{i,AoA}$. Similarly, let g_i^k be the wave amplitude of the kth subpath of the ith path defined by the departure angle $\phi_{i,AoD}^{k}$. With these definitions a mathematical representation of the cross-polarized channel can be obtained from the result for the co-polarized channel in [25]. This is given by:

$$\begin{aligned} h_{su}^{pq}(t) = \lim_{N\to\infty} \lim_{M\to\infty} \sum_{i=1}^{N} g_i \left\{ \sum_{k=1}^{M} g_i^k \Psi_i^k exp\left(-\frac{j2\pi d_{si}^k}{\lambda}\right)\right\} \\ exp\left(-\frac{j2\pi d_{iu}}{\lambda} + j2\pi f_D \cos(\phi_{i,AoA} - \phi_v)t\right) \end{aligned} \tag{32}$$

where

$d_{si}^k = k$th distance between BS antenna s and scatterer S_i
$d_{iu} =$ distance between scatterer S_i and MS antenna u
$\phi_v =$ angle of mobile direction

In the co-polarized model $\Psi_i^k = \exp(j\psi_i^k)$ and represents the phase shift of the subpath. In the cross-polarized case, there are four phase shift terms corresponding to the four polarizations (VV, VH, HV, HH). In addition, the power of each polarization is affected by the antenna slant offset angles, the XPDs and the angles of the rays relative to the array broadside [1], [26]. Therefore we define Ψ_i^k for the cross-polarized case as

$$\begin{aligned}\Psi_i^k = &\cos(\alpha_p)\cos(\alpha_q)\exp(j\psi_i^{k,VV})+\\ &\sqrt{r_{i1}^k}\cos(\alpha_p)\sin(\alpha_q)\cos(\phi_{MS}-\phi_{i,AoA})\exp(j\psi_i^{k,VH})+\\ &\sqrt{r_{i2}^k}\sin(\alpha_p)\cos(\alpha_q)\cos(\phi_{BS}-\phi_{i,AoD}^k)\exp(j\psi_i^{k,HV})+\\ &\sin(\alpha_p)\sin(\alpha_q)\cos(\phi_{BS}-\phi_{i,AoD}^k)\cos(\phi_{MS}-\phi_{i,AoA})\exp(j\psi_i^{k,HH})\end{aligned} \tag{33}$$

Assuming a von-Mises distribution for the angles at both BS and MS ends, the power of every path or subpath is given by

$$\begin{aligned}(g_i)^2 &= \frac{\exp[\kappa_{MS}\cos(\phi_{i,AoA}-\bar{\phi}_{AoA})]}{2\pi I_0(\kappa_{MS})}d\phi_{i,AoA}\\ (g_i^k)^2 &= \frac{\exp[\kappa_{BS}\cos(\phi_{i,AoD}^k-\bar{\phi}_{i,AoD})]}{2\pi I_0(\kappa_{BS})}d\phi_{i,AoD}^k\\ &\approx \frac{\exp[\kappa_{BS}\cos(\phi_{i,AoD}^k-\Delta\sin(\phi_{i,AoA}))]}{2\pi I_0(\kappa_{BS})}d\phi_{i,AoD}^k\end{aligned} \tag{34}$$

The approximation in (34) is valid when $\Delta = R/D$ is small and R and D are the radius of the scatterer ring and the link distance respectively.

The parameters in (34) have the following physical interpretation. $\bar{\phi}_{AoA}$ represents the direction of the strongest incoming wave seen by the MS. Similarly, $\bar{\phi}_{i,AoD}$ is the direction of the strongest incoming wave seen from a specified scatterer S_i, which can be determined by $\phi_{i,AoA}$. Moreover, κ governs the angle spread, more specifically $4/\sqrt{\kappa}$ is the 95% angle spread. At the MS, κ_{MS} relates to the path angle spread whereas at the BS, κ_{BS} relates to the subpath angle spread. Equation (34) also shows that each AoA is associated with one particular mean angle of a cluster of subpaths. κ_{BS} can control the spread of the subpath and determine the correlation between AoA and AoD. The higher value of κ_{BS}, the higher the correlation between AoA and AoD.

Substituting (32) in $\rho_{su,s'u'}^{pq,p'q'} = E[(h_{su}^{pq})(h_{s'u'}^{p'q'})^\dagger]$ and then using the von Mises assumptions (34), we have a correlation involving double integrals. For this reason we prefer to investigate approximations based on the series expansion $\exp\{\kappa_{BS}\Delta\sin(\theta_{i,AoA})\sin(\theta_{i,AoD}^k)\} \approx 1+\kappa_{BS}\Delta\sin(\theta_{i,AoA})\sin(\theta_{i,AoD}^k)$. The zeroth-order approximation takes only the first term (unity) in the series expansion. Now the double integral after using the zeroth-order approximation can be separated into four integrals which lead to the sum of four spatial correlation terms and can expressed as a matrix form shown in (10). A first order approximation results from taking the first two terms and also gives a sum-Kronecker from although more complex [27].